AD-A145 793 ELECTROCHEMICAL IMPREGNATION OF NICKEL COMPOSITE ELECTRODES(U) NAVAL SURFACE WEAPONS CENTER SILVER SPRING MD A L LEE ET AL. 01 AUG 82 NSWC/TR-82-414 1/1

UNCLASSIFIED F/G 7/4 NL

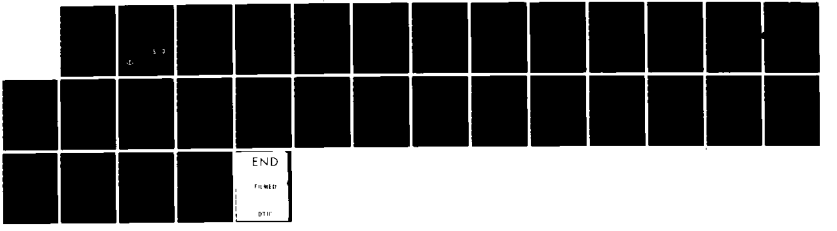

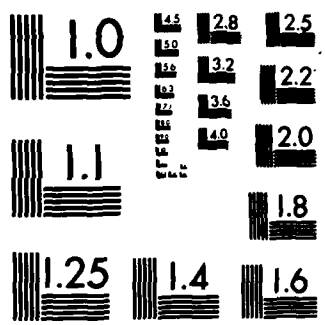

NSWC TR 82-414

AD-A145 793

DTIC FILE COPY

ELECTROCHEMICAL IMPREGNATION OF NICKEL COMPOSITE ELECTRODES

BY A. L. LEE W. A. FERRANDO F. P. FLIGHT

RESEARCH AND TECHNOLOGY DEPARTMENT

1 AUGUST 1982

Approved for public release, distribution unlimited

NAVAL SURFACE WEAPONS CENTER

Dahlgren, Virginia 22448 • Silver Spring, Maryland 20910

UNCLASSIFIED

SECURITY CLASSIFICATION OF THIS PAGE *(When Data Entered)*

REPORT DOCUMENTATION PAGE	READ INSTRUCTIONS BEFORE COMPLETING FORM
1. REPORT NUMBER: NSWC TR 82-414	2. GOVT ACCESSION NO.: A145 793
	3. RECIPIENT'S CATALOG NUMBER:
4. TITLE *(and Subtitle)*: ELECTROCHEMICAL IMPREGNATION OF NICKEL COMPOSITE ELECTRODES	5. TYPE OF REPORT & PERIOD COVERED: Interim Technical Report '80, '81
	6. PERFORMING ORG. REPORT NUMBER:
7. AUTHOR(s): A. L. Lee, W. A. Ferrando, F. P. Flight	8. CONTRACT OR GRANT NUMBER(s):
9. PERFORMING ORGANIZATION NAME AND ADDRESS: Naval Surface Weapons Center, White Oak Laboratory, Silver Spring, MD 20910	10. PROGRAM ELEMENT, PROJECT, TASK AREA & WORK UNIT NUMBERS: 62761N, F61545, SF61-545-601, 2R32BH
11. CONTROLLING OFFICE NAME AND ADDRESS:	12. REPORT DATE: 1 August 1982
	13. NUMBER OF PAGES: 31
14. MONITORING AGENCY NAME & ADDRESS *(if different from Controlling Office)*:	15. SECURITY CLASS. *(of this report)*: UNCLASSIFIED
	15a. DECLASSIFICATION/DOWNGRADING SCHEDULE:

16. DISTRIBUTION STATEMENT *(of this Report)*

Approved for public release; distribution unlimited.

17. DISTRIBUTION STATEMENT *(of the abstract entered in Block 20, if different from Report)*

18. SUPPLEMENTARY NOTES

19. KEY WORDS *(Continue on reverse side if necessary and identify by block number)*

IMPREGNATION
COMPOSITE PLAQUE
NICKEL ELECTRODE
ELECTROCHEMICAL IMPREGNATION

20. ABSTRACT *(Continue on reverse side if necessary and identify by block number)*

The nickel composite electrode (Ni.C.E.) is under development at the Naval Surface Weapons Center. The electrode demonstrates advantages over conventional nickel powder sintered electrodes in being light-weight, possessing high strength, and having a wide range of porosity.

DD FORM 1 JAN 73 1473 EDITION OF 1 NOV 65 IS OBSOLETE
S/N 0102-LF-014-6601

UNCLASSIFIED

SECURITY CLASSIFICATION OF THIS PAGE *(When Data Entered)*

20. (Cont.)

The nickel composite electrode is made by coating mats of graphite fiber with electroless nickel. A nickel coated mat is much lighter when used in an electrode than the customary nickel powder for a given material volume. A nickel wire grid is sandwiched between several such mats and sintered under compression to the desired thickness.

While maintaining sufficient electrical conductivity, the resulting plaque is lightweight, durable and highly porous. Variation of compaction pressure or graphite fiber content produces porosity in the range of 60% to 90%. The open composite plaque pore structure allows easy active material deposition.

The nickel hydroxide active material was loaded into the electrode plaque by electrochemical impregnation. An ethanol-based nitrate impregnating solution was employed. Optimum impregnations were achieved using a constant current density of 0.058 amperes/cm^2(0.374 amps/in^2) of electrode surface.

Composite electrodes fabricated for this study routinely achieved energy densities of 170 amp hours/kilogram (Ah/Kg) at a C/2 discharge rate to 0.5 V. cutoff. Use of the composite electrode in Ni-Cd cells will increase their gravimetric energy density 40% above available commercial cells.

FOREWORD

The objective of this study was to explore the application of the electrochemical impregnation technique to the nickel composite electrode (Ni.C.E.). The impregnating conditions examined include current density, current frequency, and loading level. In addition, various electrode characteristics which affect performance were studied. These characteristics were thickness, porosity, and resistivity.

Performance of the nickel composite electrode was determined to be superior to that of commercially available powder sintered electrodes on a gravimetric basis. Ni.C.E. achieves energy densities over 170 Ah/Kg at C/2 discharge rates. The active material utilization exceeded 100 percent. Commercial powder sintered electrodes, by comparison, achieve about 110 Ah/Kg. Volumetric energy densities at present are comparable for Ni.C.E. and commercial sinters.

The most efficient impregnation and best morphology of active material, fine black crystals, was obtained using a direct current density of 0.058 amperes/cm^2 (0.374 amps/in^2).

Eighty-one percent void volume and 40 mil (1 mm) thickness were the optimal composite plaque substrate characteristics, as determined by comparing energy density and active material utilization of the finished electrodes in cycling tests.

Approved by:

J. R. Dixon

JACK R. DIXON, Head
Materials Division

CONTENTS

ILLUSTRATIONS

TABLES

INTRODUCTION

The nickel electrode is the backbone of an entire class of alkaline secondary cells including the Ni-Cd, Ni-Fe, Ni-Zn and Ni-H_2 systems. The most successful nickel electrode for many purposes has been the sintered type. Sintered nickel electrodes have been made conventionally for many years from fine nickel powders. While these electrodes have amply proven themselves in many applications, there continues to remain a need for improved energy density at reduced fabrication costs.

The nickel composite electrode[1] (Ni.C.E.) has been under development at NSWC for several years. The composite substrate was fabricated by electroless nickel coating[2] graphite mat fiber material and sintering under compaction pressure. While maintaining sufficient electrical conductivity, the resulting plaque is lightweight, durable and highly porous (55 to > 90 percent). The active material, nickel hydroxide was loaded into the plaque by an electrochemical impregnation method developed and reduced to practice by Pickett.[3]

In order to produce a successful electrode, each step of the fabrication operation must be understood and each parameter must be carefully controlled. The general objectives of this report are the documentation of the major fabrication processing steps and preliminary study of several important parameters. In particular, the nickel coating procedure is described in some detail. Impregnation current density, frequency of applied current and active material loading level, each controllable in the impregnation phase, are examined for their contribution to electrode utilization. Finally, the effects of various plaque parameters: thickness, porosity and resistivity on electrode performance are studied by means of extensive cycling tests.

EXPERIMENTAL METHOD

Each graphite mat was uniformly coated with nickel prior to compression and sintering. After initial cutting and weighing, the mat was soaked in hot (100°C) deionized water. Care was taken to ensure that the mat remained undamaged and free of clinging air bubbles. The surface was cleaned by immersion in dilute hydrochloric acid. After soaking for 5 minutes in the dilute hydrochloric acid, the mat was transferred directly to the catalyst solution for a similar period. In each of these soaking operations, the mat was

compressed gently in order to allow the solution to penetrate the fibers completely. The catalyst provides sites which promote precipitation of nickel from the coating solution [catalyst, accelerator, electroless nickel solutions from Allied-Kelite Division, Richard Chemical Co.]. After double rinse in deionized water, the mat was immersed in an accelerator solution (50-65°C) for 5 minutes and again rinsed twice in deionized water. For each mat, 600 ml of the nickel coating solution were used. This amount is sufficient to produce a 0.5μ coating on a 1 gram mat for an immersion time of about 1 hour. Often, this step must be repeated in order to obtain coating thickness between 0.6 and 0.8μ. Optimal coating bath temperature was found to be 80 to 84°C.

After incorporating several flipping and compressing techniques, an optimal method for ensuring complete coating was developed. By leaving the mats on the surface of the solution and flipping them periodically (once every 2 minutes), a uniform nickel coating was achieved. If the mats are constantly compressed and flipped and forced to remain submerged, the reaction rate is accelerated to an unacceptable level. The solution eventually turns gray and nickel is coated onto the container. It is believed that small slivers of carbon thrown off the mat during aggressive flipping and compression act as nucleation sights for the reaction, in turn causing a runaway situation.

Upon completion of the coating process, the mats were removed from the expended solution. After a double rinse in deionized water and an acetone rinse, they were allowed to air dry for a period of 1 to 2 hours. Completely dry nickel coated mats appear grayish silver in color and provide a lightweight, compressible and sinterable substrate. Occasionally a mat will display light brown patches, however, this does not seem to affect the sintering process or the performance of the plaque. It is very important that the mats be completely and evenly coated and that no small uncoated spots remain. If the mats have uncoated spots, the final sinter will be weak and blister prone.

In order to obtain a properly conducting substrate, 0.6 to 0.8μ (1μ = 10^{-6} meters) of nickel must be deposited on the fibers. This can be equated roughly to a final (after coating) mat weight of about three times its initial weight. The sintering process itself and measurements on the Ni.C.E. plaques for porosity, resistivity and tensile strength have been reported previously.[4] A wide range of porosity (55 to 90 percent) is achievable by varying the fiber density. The open pore structure of the composite allows efficient impregnation of the active material.

PARAMETERS AND CONDITONS OF DATA ACQUISITION

Data was acquired in two stages. In stage one, three impregnating conditions, current frequency, current density, and loading level were chosen as variables. A statistical method of analysis, the Box Behnken Plan,[5] was used to evaluate the results. In stage two, the best conditions resulting from the Box Behnken Plan were used to study additional parameters--thickness, porosity, and resistivity, which affect performance of the electrode.

IMPREGNATION OF THE ELECTRODE PLAQUE

A schematic of the electrochemical impregnation process is shown in Figure 1. The process consists of impregnation and then formation of the electrode plaque. Figure 2 shows the impregnation cell with plaque and nickel counter-electrodes (anodes) in place. This cell is immersed in the impregnation bath.

The impregnation conditions examined are listed in Table 1. Three trials were made for each condition.

TABLE 1. IMPREGNATION CONDITIONS

Current Frequency	Current Density	Loading Level
direct current	0.106 amps/cm^2	2.0 grams
0.33 pulses/sec	0.058 amps/cm^2	1.5 grams
10 pulses/sec	.029 amps/cm^2	1.0 grams

Electrodes were impregnated using a combination of the three above conditions.

The electrode plaque (dimensions 2 3/4" x 1 3/4") acted as a cathode in the center slot of the impregnating cell (see Figure 2) between consumable nickel anodes.

The impregnating solution consisted of 1.8 M (93 wt/o) nickel nitrate ($Ni(NO_3)_2$) and 0.135 M (7 wt/o) cobalt nitrate ($Co(NO_3)_2$) in a 50-50 ethanol-water mixture. Control of the solution pH around 2.5 was found to be very important. This fact will be discussed later. Solution temperature was maintained between 75° and 80°C.

FORMATION OF ELECTRODE

Following impregnation, the plates were formed. The formation process reduces residual nitrates into ammonia and cleans the surface of the electrode. It also appears to redistribute the active material by helping to unblock small pores. The electrolyte was 20 percent KOH. The formation consisted of: (1) a 20 minute cathodization period and (2) polarity reversal (anodization) for another 20 minutes. This process was repeated three times. The current applied for each period is indicated in Table 2. For some trials, the initial cathodization period was extended to 2 hours.

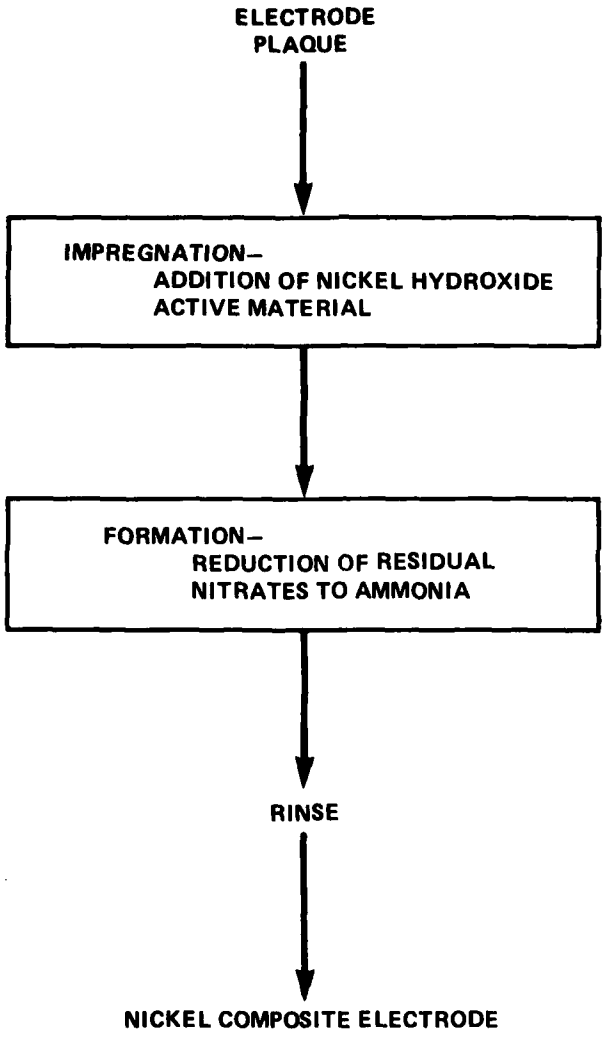

FIGURE 1. THE ELECTROCHEMICAL IMPREGNATION PROCESS

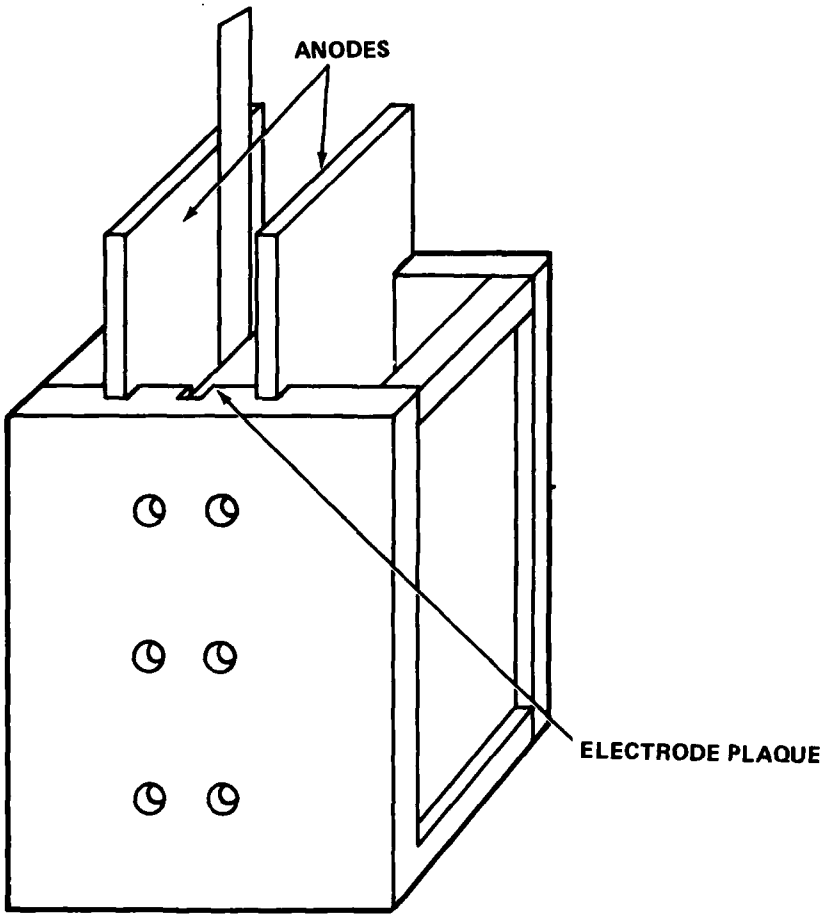

FIGURE 2. IMPREGNATION CELL

TABLE 2. ELECTRODE FORMATION PROCESS IN 20 PERCENT KOH SOLUTION

Cycle	1	2	3	4
Applied Current	0.070 amps/cm^2 (0.45 amps/in^2)	0.070 amps/cm^2 (0.45 amps/in^2)	0.0155 amps/cm^2 (0.10 amps/in^2)	0.0109 amps/cm^2 (0.07 amps/in^2)

After formation, the electrodes were thoroughly rinsed in circulating deionized water. Each electrode was dried and weighed. The C rate was determined from the dry active material weight in the electrode using the electrochemical equivalent for nickel of .289 Ah/gram.

TESTING OF ELECTRODE

A single impregnated composite electrode was sandwiched between commercial cadmium negatives. The number of negatives was chosen to provide a positive limiting condition. Each positive was wrapped in a single layer of nylon and permion [Permion Division, RAI Research Corp., Hauppauge, L.I., N.Y.]. The stack was inserted into a chemically resistant plastic case containing 32 percent KOH electroylte with no additives, under flooded conditions. The continuous test regime included discharge (DOD 95 percent) at the C and C/2 rates, respectively, performed by automatic cycling devices in a constant current mode. Charging was carried out at the C rate in all cases.

DATA AND RESULTS

Part I

Impregnating conditions of current frequency, current density, and loading level were studied. The three variables were examined by the Box Behnken Plan. This statistical method of analysis allowed three independent variables to be studied by plotting middle-of-the-edge points. This method minimized the number of trials required for statistical confidence. The trials were plotted according to the Box Behnken Plan on a three dimensional graph (see Figure 3). Variables of current frequency, current density, and loading level are plotted along the X, Y, and Z axes respectively. Active material utilization to .5 volts and .9 volts discharge cutoff respectively are indicated.

From the Box Behnken test, active material utilization results indicated that the best impregnating condition was a direct current density of 0.058 amps/cm^2 and high loading levels, 1.5 to 2.0 grams. Active material utilization in the direct current trials was higher than that at .33 pulses/sec. There was

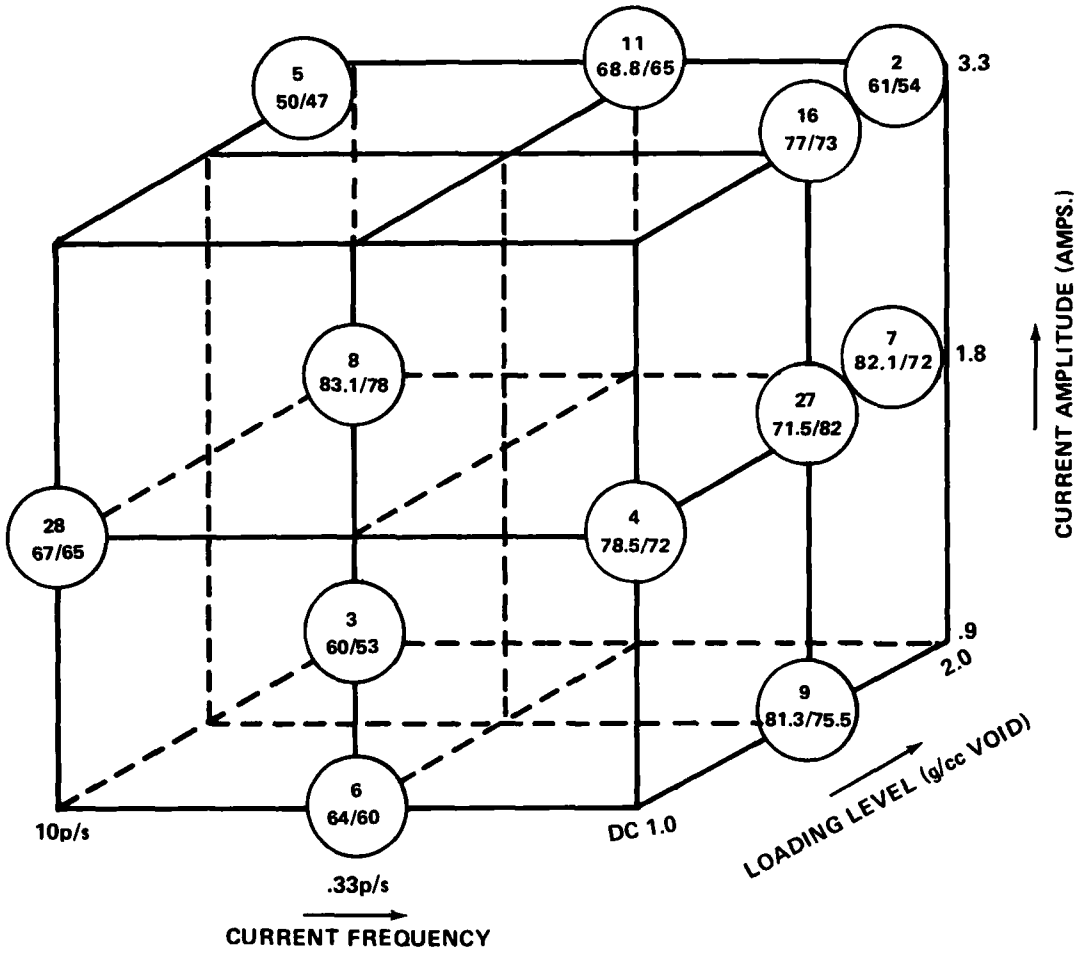

UTILIZATIONS TO 0.5 AND 0.9 VOLTS DISCHARGE CUTOFF ARE INDICATED, RESPECTIVELY:

ELECT#
0.5/0.9

FIGURE 3. BOX BEHNKEN PLAN IMPREGNATION TRIALS

no significant difference in utilization between direct current and 10 pulses/second. Having made these observations on the relative efficiency of pulsed current, direct current was the optimal choice for current frequency.

Current density of 0.058 amps/cm^2 resulted in the best form of active material. The low current, 0.029 amps/cm^2, was observed to plate nickel onto the electrode plaque. High current, 0.106 amps/cm^2, loaded the plaque with green hydrated form of nickel hydroxide. The best current density of 0.058 amps/cm^2 resulted in black, evenly distributed active materi..

High plaque loading levels were found to be desirable because of the measured higher energy densities.

Part II

Part II of the experiment involved studying the effects of electrode physical characteristics--thickness, porosity, and resistivity on performance by using the current settings determined from Part I. Individual parameters were evaluated by studying the cycling tests data, comparing utilizations and energy densities.

From the cycling test data, the performance and quality of the electrode were evaluated. Data on electrode #41 is shown at 50 cycle intervals in Figure 4. The set of curves shows the changes in charge-discharge profile shape as the composite electrode is cycled.

Utilization at .5 volts and .9 volts discharge cutoff were calculated from the cycling test data and plotted. Figure 5 displays the utilization curve of electrode #41, active material utilization versus number of cycles. The corresponding energy density is indicated along the right edge of the graph. The utilization curve of electrode #46 is shown in Figure 6. The respective electrode characteristics and impregnation conditions are listed in Table 3.

Individual electrode characteristics were studied for their effects on performance. Electrodes of two thicknesses were tested. Table 4 reports the thickness, loading level, utilization, and energy density for electrodes #46 and #48 (0.64 mm thick) and electrodes #41, #53, and #38 (1.0 mm thick). Electrodes with porosities ranging from 60% to 80% were examined. Table 5 compares the effects of porosity on loading level, utilization, and energy density. The resistivity of the electrode also affected electrode performance as shown in Figure 7. A graph of percent utilization versus resistivity is presented.

Impregnation trials were made in a pure water solution containing 2.0 M nickel nitrate, 0.1 M cobalt nitrate and 3.0 M sodium nitrate. The results are listed in Table 6. Electrodes impregnated in aqueous solution performed poorly. Utilization was only 75.5 percent for electrode #23 and 62 percent for #52, respectively, corresponding to energy densities of only 116 Ah/Kg and 88.5 Ah/Kg. These results may be compared with those of Tables 4 and 5 for ethanol based impregnations, where utilizations exceeding 100 percent were common under similar test conditions. The presence of ethanol in the impregnating bath serves several purposes: it reduces the nickel nitrate solution surface tension, allowing easier penetration into the composite plaque; it acts as a buffer in helping to stabilize the pH within the pore structure.

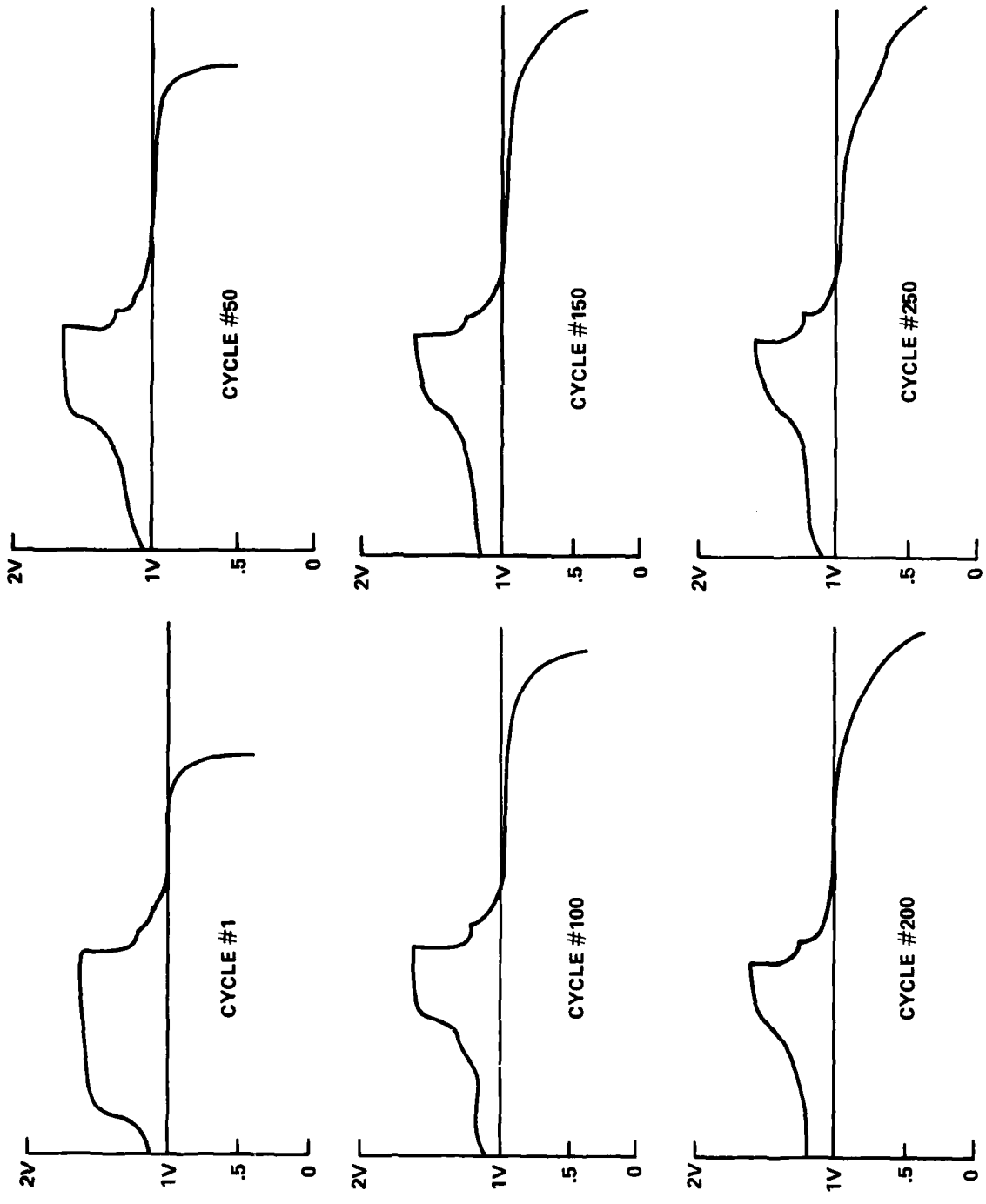

FIGURE 4. CYCLING TEST DATA, ELECTRODE #41

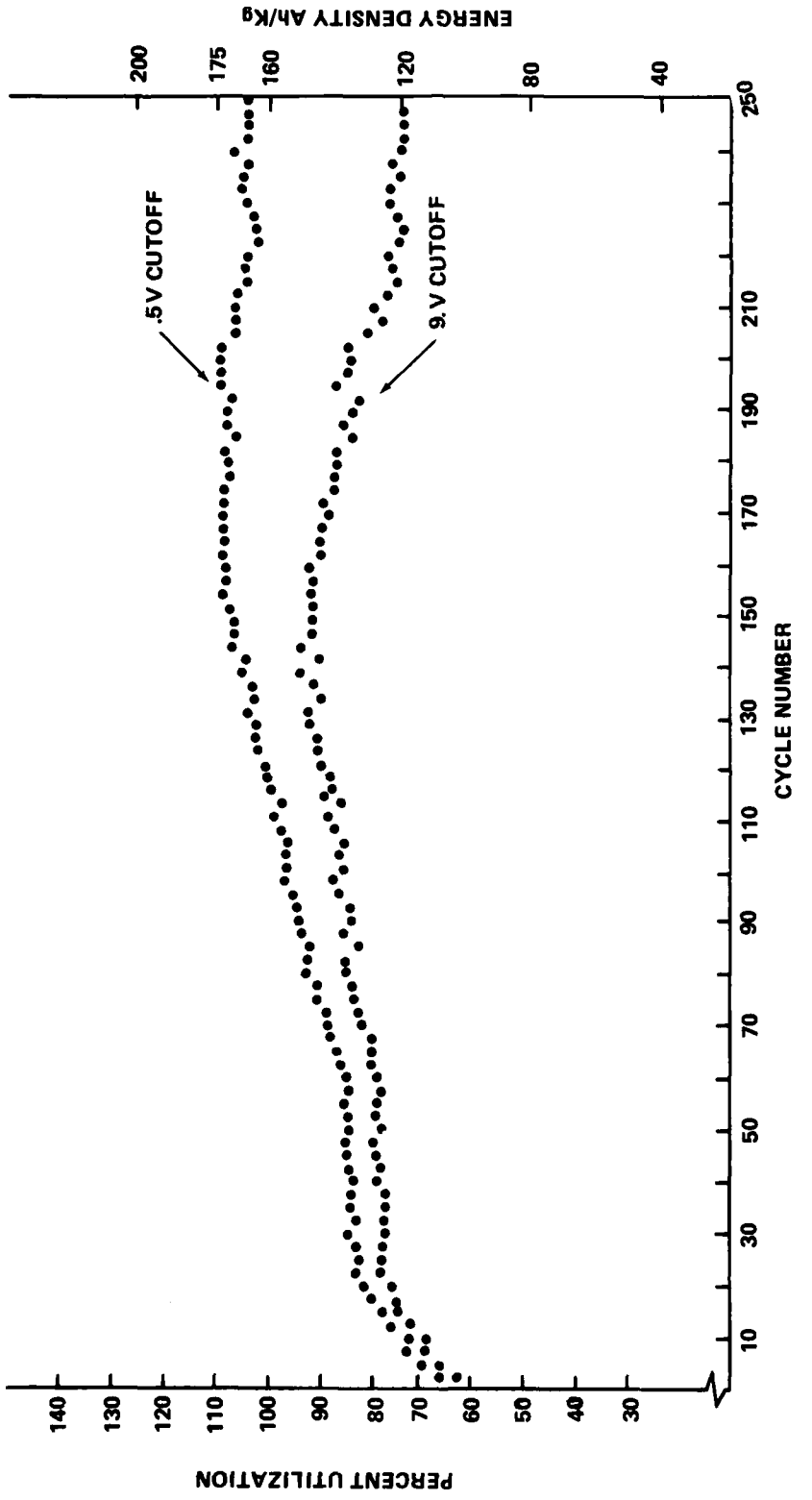

FIGURE 5. UTILIZATION VERSUS CYCLE NUMBER, ELECTRODE #41

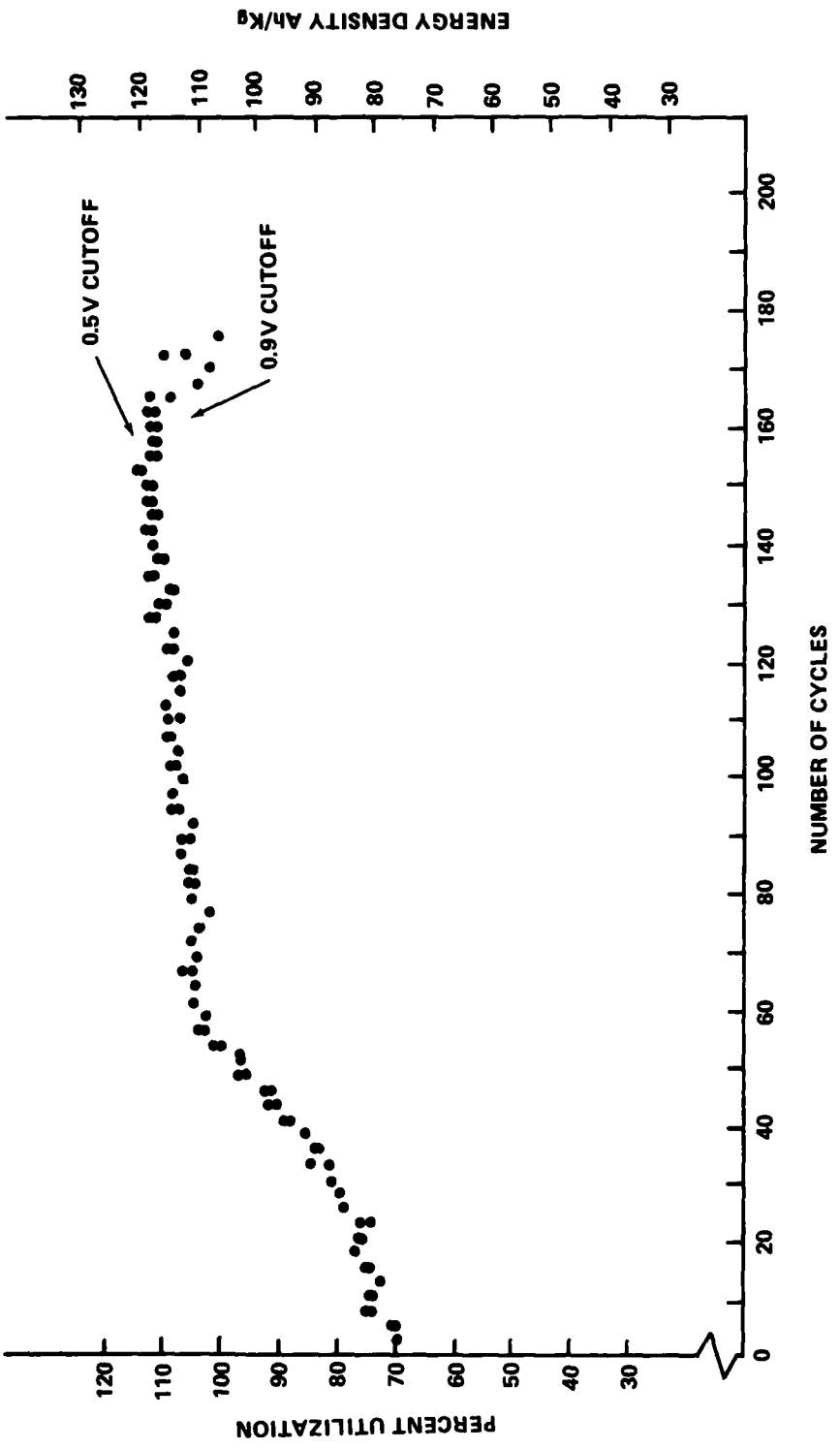

FIGURE 6. UTILIZATION VERSUS CYCLE NUMBER, ELECTRODE #46

TABLE 3. TEST ELECTRODE PARAMETER SUMMARY

ELECTRODE #	POROSITY %	THICKNESS CM	RESISTIVITY $\mu \cdot \Omega \cdot CM$	IMPREGNATION CURRENT FREQUENCY	IMPREGNATION CURRENT AMPS.	LOADING LEVEL g/cc VOID	ACTIVE MATERIAL UTILIZATION %	ENERGY DENSITY Ah/Kg
22	81.9	0.109	1157.3	DC	1.8	1.06	–	–
23	83.1	0.106	1009.6	AQUEOUS SOLN. DC	1.8	1.22 *	72.5	116.0
31	81.8	0.107	1091.5	10 PULSES/SEC	0.9	1.37 *	79.4	128.3
35	83.3	0.103	1074.4	.33 PULSES/SEC	1.8	1.09	43.8	64.1
37	81.7	0.121	1274.6	DC	3.3	1.61	73.0	126.7
38	81.6	0.119	1219.9	DC	1.8	1.43 *	100	170.0
40	81.5	0.112	843.2	DC	1.8	0.796	63.1	72.4
41	81.4	0.109	954.2	DC	1.8	1.37	109.5	173.9
42	81.9	0.110	1397.8	DC	1.8	0.798	82.0	76.5
43	77.6	0.106	1038.3	REPEATED IMPREG. DC	1.8	1.53	78.1	121.9
44	78.4	0.109	1066.4	10 PULSES/SEC	1.8	1.12	70.0	97.1
45	78.2	0.108	878.4	DC	0.9	0.877	23.1	36.1
46	77.2	0.062	710.4	DC	1.8	1.18 *	116.3	123.1
47	75.0	0.054	532.1	DC	1.8	1.50 *	96	108.7
48	64.3	0.066	540.3	DC	1.8	1.208	121.5	110.6
52	80.8	0.107	677.6	AQUEOUS SOLN. DC	2.4	1.33 *	62.0	88.5
53	80.6	0.106	749.9	DC	1.8	1.21 *	100.8	145.3

*LONG FORMATION PROCESS

TABLE 4. EFFECT OF ELECTRODE THICKNESS ON PERFORMANCE

Electrode No.	Thickness cm.	Loading Level g/cc Void	Utilization %	Energy Density Ah/Kg
48	0.006	1.208	121.5	110.6
46	0.062	1.18	116.3	123.1
41	0.109	1.37	109.5	173.9
53	0.106	1.24	100.0	145.3
38	0.119	1.43	100.0	170.0

TABLE 5. EFFECT OF POROSITY ON ELECTRODE PERFORMANCE

Electrode No.	Porosity %	Loading Level g/cc Void	Utilization %	Energy Density Ah/Kg
48	64.3	1.208	121.5	110.6
46	77.2	1.18	116.3	123.0
41	81.4	1.37	109.5	173.9
38	81.6	1.43	100.0	170.0

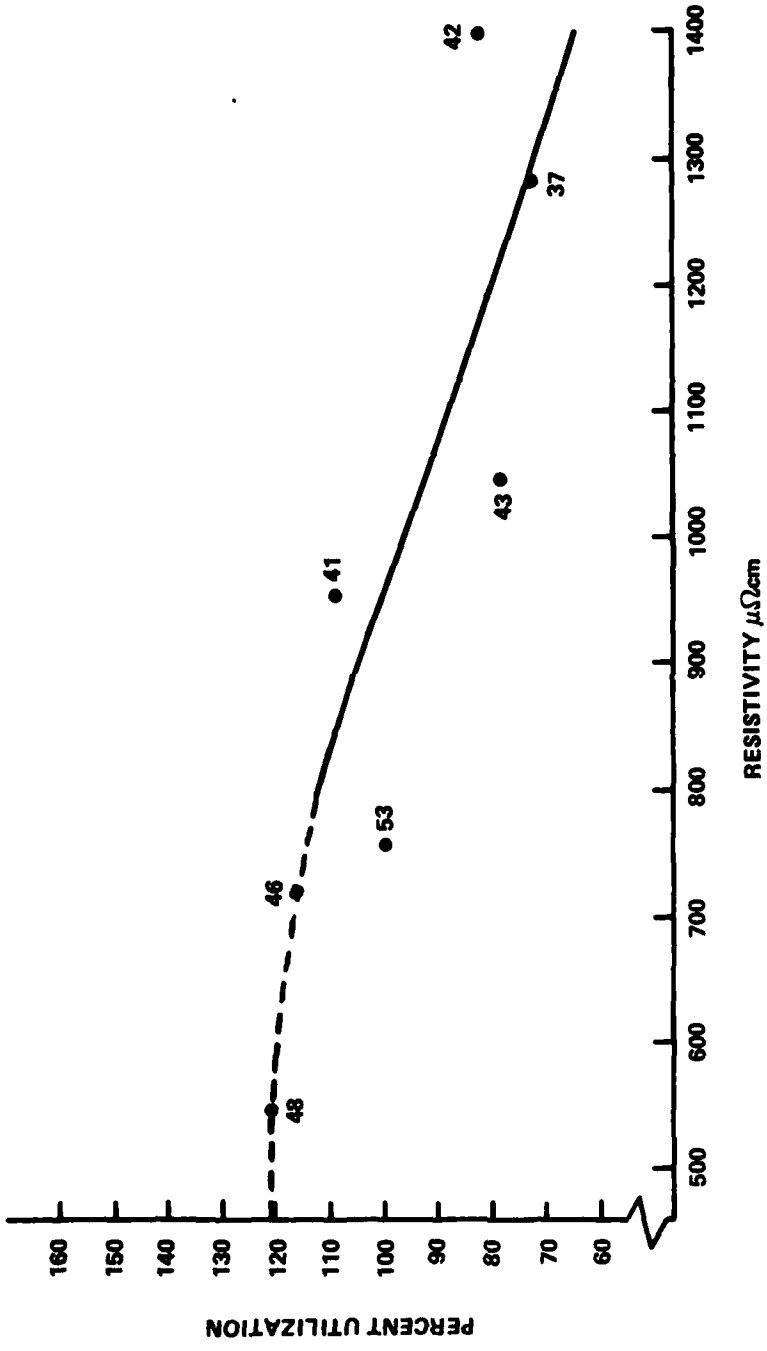

FIGURE 7. UTILIZATION VERSUS PLAQUE RESISTIVITY

TABLE 6. AQUEOUS SOLUTION RESULTS

Electrode No.	Porosity %	Thickness cm.	Loading Level g/cc Void	Utilization %	Energy Density Ah/Kg
23	83.2	0.106	1.22	72.5	116.0
52	80.8	0.107	1.33	62.0	88.5

DISCUSSION

The optimal impregnating conditions of current frequency, current density and loading level were studied. The current frequencies ranged from constant pulse (direct current) to 10 pulses/second. It has been suggested[6] that long duration pulses may increase the loading capacity by allowing a replenishing of the nickel ion concentration in the solution within the pores during the "off" period. Such pulses of 5 to 10 minutes duration were not included in this impregnation study. This condition will be tested in future work for comparison of results with those of constant current impregnation.

Figure 3, a three dimensional graph of the impregnated conditions plotted according to the Box Behnken Plan, does not fully satisfy the middle of the edge points prescribed by the Plan. The Box Behnken Plan assumes only three independent variables, but throughout the test it became apparent that there were numerous parameters affecting the impregnation. It was difficult to hold all other parameters constant while testing for only three. Since the electrode plaques were manufactured on a laboratory bench scale, it was difficult for all electrodes to be made uniformly. Also, the loading level of 1.0, 1.5, and 2.0 grams were not exactly achievable as predicted from theoretical calculations. In spite of the experimental difficulties, there appears to be a direct relationship between theoretical and experimental results. From the Box Behnken Plan test, delineations could be drawn indicating the best conditions for impregnation. These conditions are presented in the Conclusions.

Interpretation of Cycling Data

Figure 8 contains schematic representations of charge/discharge curves for the nickel-cadmium electrode couple. Information on electrode efficiency can be obtained by examining these curve shapes. The top picture in Figure 8(a) represents the nickel charging cycle. The charging takes place with a monotonic increase in potential. The cadmium charge cycle, 8(b), shows that a sharp rise in potential occurs as the electrode reaches full charge. The addition of both nickel and cadmium charge cycles results in the cycle as shown in Figure 8(c). Region A represents overpotential, the rise in potential required to sustain charging. Region B, the plateau region, is the actual charging of the cell. The exhaustion, Region C, occurs as charging is completed. The rise in

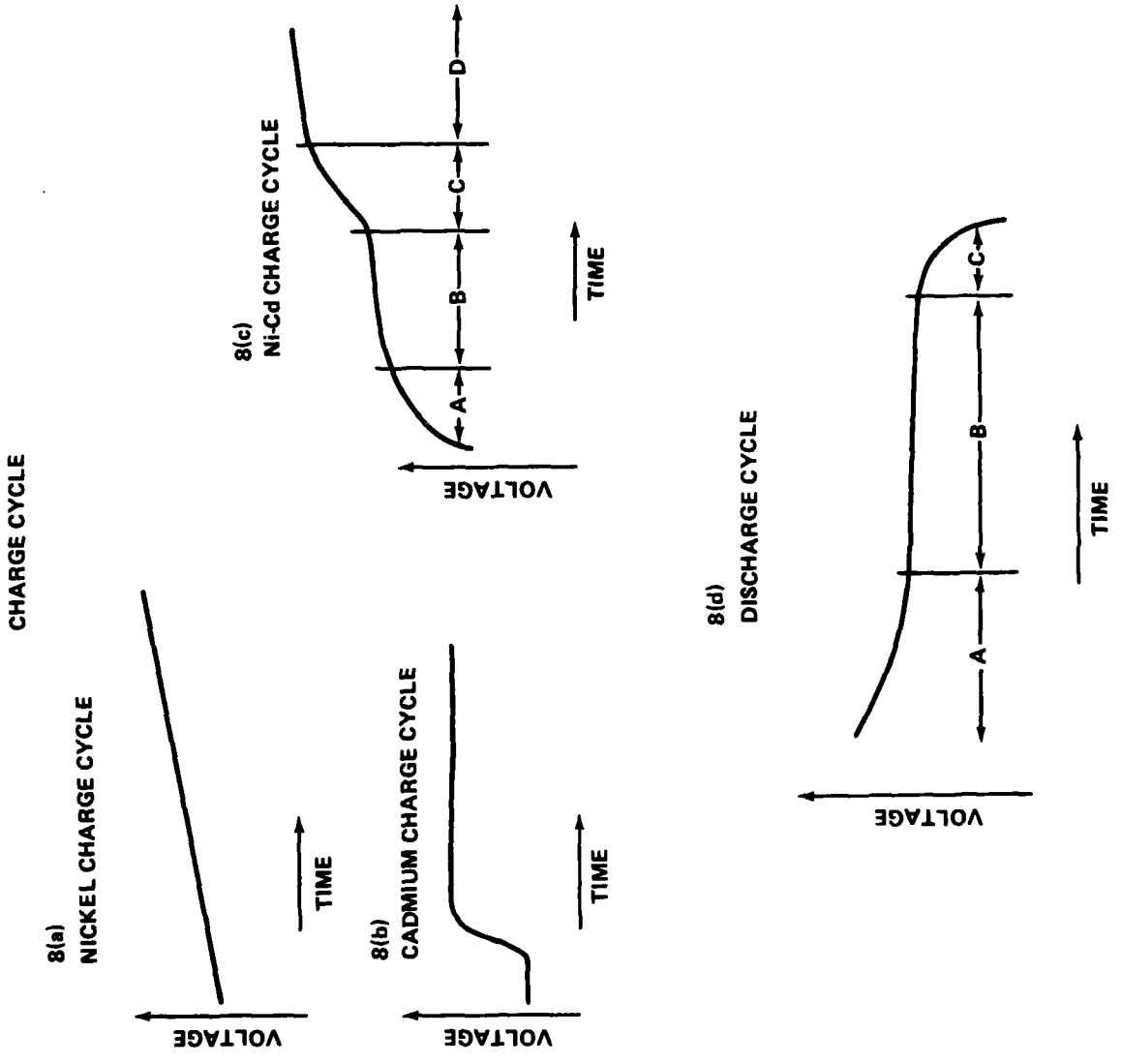

FIGURE 8. CHARGE-DISCHARGE POTENTIAL PROFILES

potential indicates an increase in resistivity as the active material becomes fully charged. Region D is known as overcharge; oxidation is occurring at the electrode. The discharge of a Ni-Cd battery is portrayed in the lower half of the figure. Region A displays a decrease in potential due to a change in the concentration of the active material. The steady state Region B represents the cell discharging. Region C, the knee of the curve, is the exhaustion region. This drop in overpotential is due to the decrease of reactant from charged to discharged state. If the drop is sharp, the change in potential is due to the decrease of available charged material, but if the decrease in potential drop is slow and sloping, then the potential drop occurs because of increasing resistivity.

Actual cycle data for electrode #41 of Figure 4 may be analyzed as an example. The plateau region of the charge cycle becomes progressively longer with cycling. The exhaustion region rises to a steeper slope. The longer plateau region indicates that the nickel electrode is retaining more charge. The sharp rise and short plateau of the exhaustion region represents charge completion in the cadmium electrode, indicating that the nickel and cadmium electrode are quite well matched in capacity. A sharp drop in the potential at the end of the discharge cycle occurs. This is an example of the condition mentioned above where the potential drop is due to decrease in charged active material. The deteriorating potential drop of the discharge exhaustion region with increasing cycle number is evident. A semiconducting layer of unchargeable active material, through which the current must pass, builds up with cycling. This layer increases electrode resistivity, markedly altering the discharge curve shape, especially below 0.9 volts.

Life Cycle Utilization Profiles

Figure 5 displays a life cycle utilization profile of electrode #41. This profile is also representative of other electrodes. There are common characteristics of these curves (see also Figure 6). A region of increasing utilization extends for about 30 cycles and then the utilization levels off for another 30 to 40 cycles. At about cycle 70, another region of increasing utilization results followed by a plateau region near 100 percent efficiency.

An attempt was made to eliminate the region of increasing utilization. Based on a suggestion by H. N. Seiger, an extended formation process was used. The initial cathodization period was extended for 2 hours. Results suggested that the long formation process prepared the active material to a similar degree as did the first 50 cycles. Initial utilization was somewhat improved but the entire region of increasing utilization could not be eliminated.

Effects of Electrode Characteristics on Impregnation

Thick electrodes (40 mils) were found to attain greater energy densities than thin electrodes. The amount of active material loaded in a thin electrode was limited by the relatively large current collector volume. Conversely, active material and thus greater energy density is realized in thick electrodes due to the presence of a relatively larger sinter body. However, a too thick electrode may encounter problems with unevenly distributed active material and

higher resistivity. High porosity (80 percent) electrodes were determined to be more favorable by the same reasoning. Electrodes too porous (>90 percent) have larger average pore size and decreased electrical conductivity, adversely affecting electrode performance. The resistivity was lowered for electrode #53 by adding strips of current collector diagonally across each side of the grid. But, the added weight of the strips made the electrode plaque heavier. Consequently the gravimetric energy density was reduced.

Role of pH

Another factor which greatly affects the impregnation is the pH of the impregnation solution. Higher loading levels were achieved with acidic solutions; however, high acidity (low pH) also promotes corrosive attack of the sinter matrix. It is recommended, therefore, that the pH be maintained around 2.5 with an automatic pH controller. At about pH 5, nickel hydroxide begins to precipitate out of the solution. The active material is no longer available for loading into the plaque. In addition, the precipitate forms a surface buildup which blocks the pores of the electrode. An acidic bulk solution normally insures that the nickel ions reach the interior of the pores, where the OH^- is generated, before being deposted as $Ni(OH)_2$. However, as the bulk solution pH approaches 5, appreciable OH^- is present outside the plaque surface. $Ni(OH)_2$ begins to precipitate in this region. As a result, loading levels are limited in impregnation solutions of high pH.

One method tried in order to increase the loading level was to reimpregnate the electrode after formation. Electrode #43 was reimpregnated four times for 15 minutes each to see if reimpregnation enhanced electrode performance. The loading level reached 1.5 g/cc void while other electrodes impregnated for the same duration of time under single impregnation loaded to lesser levels. The electrode performance of #43 is compared with another electrode (#46) of the same porosity, and another (#41) with the same thickness. The active material utilization as well as energy density was lower in the case of reimpregnated electrodes than for the singly impregnated electrodes. Reimpregnation appears to affect the crystalline structure of the active material. Evidently the form of active material deposited by reimpregnation is not as efficient.

Comment on Utilization of Active Material

It is interesting that active material utilizations over 100 percent are achievable. This is possible since the electrochemical equivalent for Nickel is calculated assuming a pure $Ni^{2+} - Ni^{3+}$ transition. However, Ni^{4+} is also possible. In addition, differences in electrochemical activity due to the presence of cobalt have not been taken into account. The role of the cobalt additive is complex and not thoroughly understood. A study of additives in Nickel electrodes is currently underway at NSWC.

CONCLUSIONS

Performance of the nickel composite electrode is superior to that of commercially available powder sintered electrodes on a gravimetric basis. Ni.C.E. achieves energy densities of 170 Ah/Kg at C/2 discharge rates. The active material utilization approach 100 percent. Commercial powder sinters achieve about 110 Ah/Kg. Volumetric energy densities at present are comparable for NI.C.E. and commercial sinters.

The best impregnation conditions are direct current with a current density of 0.058 amps/cm^2. The optimal fine black crystalline form of active material was deposited at this current density. Pulsed current was not found to be advantageous at the frequencies employed.

Other parameters affect the performance of the electrode. These include electrode plaque characteristics--thickness, porosity, and resistivity.

Eighty-one percent porosity and 40 mil thickness were the optimal electrode characteristics determined by comparing energy density and utilization. Electrode performance increases with lower resistivity. Methods of reducing resistivity still need to be examined.

Increased loading levels are desirable since they lead to higher energy densities. But loading levels cannot be increased by reimpregnating the electrodes. These show that single impregnation yields best results. Optimum loading can occur if pH of the impregnation solution is maintained near 2.5. pH levels above 5.0 result in markedly reduced active material loading, increased surface deposition and rapid depletion of the impregnation bath.

REFERENCES

1. Ferrando, W. A., and Sutula, R. A., "Lightweight Battery Electrode," U.S. Patent No. 4,215,190, 29 Jul 1980.

2. Pushpavanam, Mrs. Malathy, and Shenoi, B. A., "Electroless Nickel, A Versatile Coating," Finishing Industries, Vol. 1, No. 6, Jun 1977, p. 48.

3. Pickett, D. F., Fabrication and Investigation of Nickel Alkaline Cells Part I: Fabrication of Nickel Hydroxide Electrodes Using Electrochemical Impregnation Techniques, Technical Report, AFAPL-TR-75-34 Part I, Oct 1975, Air Force Wright Aeronautical Laboratories, Wright-Patterson Air Force Base, Ohio 45433.

4. Ferrando, W. A., et al., Physical Properties of the Nickel Composite Sintered Plaque, NSWC TR 82-416 (to be published).

5. Box, G. E. P., Hunter, W. G., and Hunter, J. S., "Response Surface Methods," p. 510 in Statistics for Experimenters (New York: John Wiley and Sons, 1978).

6. Hardman, C. C., U.S. Patent No. 3,600,227, "Method of Impregnating Flexible, Metallic Battery Plaques," Aug 1971.

DISTRIBUTION

	Copies
Defense Technical Information Center Cameron Station Alexandria, VA 22314	12
Defense Nuclear Agency Attn: Library Washington, DC 20301	1
Pentagon Project Officer, OSD(MRA&L)-WR Attn: William G. Miller Room 2B323 Washington, DC 20301	1
Office of Deputy Under Secretary of Defense for Research and Engineering Staff Specialist for Materials and Structures Attn: Mr. Jerome Persh Room 3D1089, The Pentagon Washington, DC 20301	1
Defense Advanced Research Projects Agency Attn: E. Van Reuth L. Jacobsen 1400 Wilson Boulevard Arlington, VA 22209	1 1
Institute for Defense Analyses R&E Support Division 400 Army-Navy Drive Arlington, VA 22202	1
Library of Congress Attn: Gift and Exchange Division Washington, DC 20540	4
Office of Chief of Naval Operations Operation Evaluation Group Washington, DC 20350	1
David W. Taylor Naval Ship Research and Development Center Attn: A. B. Neild (Code 2723) W. J. Levendahl (Code 2703) J. Woerner (Code 2724) H. R. Urbach (Code 2724) D. Icenhower (Code 2721) J. Gudas (Code 2813) W. Lukens (Code 2822) Annapolis Laboratory Annapolis, MD 21402	1 1 1 1 1 1 1
Naval Air Development Center Attn: Dr. E. McQuillen Dr. G. London Warminster, PA 18974	1 1
Naval Air Systems Command Attn: Mr. R. Schmidt (Code 52031A) Washington, DC 20361	1
Naval Electronic Systems Command Attn: A. H. Sobel (Code PME 124-31) Washington, DC 20360	1

DISTRIBUTION (Cont.)

	Copies
Naval Intelligence Support Center	
Attn: Dr. H. Ruskie (Code 362)	1
4301 Suitland Road	
Washington, DC 20390	
Naval Material Command	
Attn: Code 08T223	1
J. Kelly (MAT 0725)	1
W. Holden (MAT 08E4)	1
O. J. Remson (MAT 071)	1
G. R. Spaulding (MAT 072)	1
Washington, DC 20360	
Naval Ocean Systems Center	
Attn: Code 922	1
Dr. S. D. Yamomoto (Code 513)	1
P. D. Burke (Code 9322)	1
San Diego, CA 92152	
Naval Ordnance Station	
Attn: Howard R. Paul	1
Project Manager	
Southside Drive	
Louisville, KY 40150	
Naval Postgraduate School	
Attn: Dr. William M. Tolles (Code 612)	1
Monterey, CA 93940	
Naval Research Laboratory	
Attn: Dr. Fred Saalfeld (Code 6100)	1
A. Simon (Code 6130)	1
S. C. Sanday (Code 6370)	1
I. Wolock (Code 8433)	1
H. Chaskelis (Code 8431)	1
4555 Overlook Avenue, S.W.	
Washington, DC 20375	
Naval Sea Systems Command	
Attn: M. Kinna (Code 62R4)	1
J. DeCorpo	1
E. J. Anderson	1
Code 5433	1
H. Vanderveldt (Code 05R15)	1
Code 99612	2
Code 0841B	1
Washington, DC 20362	

	Copies
Naval Underwater Systems Center	
Attn: J. Moden (Code 36123)	1
R. Lazar (Code 36301)	1
Newport, RI 02841	
Naval Weapons Center	
Attn: A. Fletcher (Code 3852)	1
China Lake, CA 93555	
Naval Weapons Support Center	
Attn: M. Robertson	1
Electrochemical Power Sources Division	
Crane, IN 47522	
Office of Naval Research	
Attn: G. Neece (Code 413)	1
B. MacDonald (Code 471)	1
G. Sandoz (Code 715)	1
J. Smith (Code 413)	1
800 N. Quincy Street	
Arlington, VA 22217	
Strategic Systems Project Office	
Crystal Mall No. 3	
Attn: G. Needham (Code 273)	1
LCDR F. Ness (Code 234)	1
LCDR H. Nakayama (Code 272)	1
Washington, DC 20362	
Army Electronics Research and Development Command	
Attn: A. Legath (Code DELET-P)	2
S. Gilman (Code DRSEL-TL-P)	1
E. Brooks (Code DRSEL-TL-P)	1
G. DiMasi (Code DRSEL-TL-P)	1
Fort Monmouth, NJ 07703	
Army Foreign Science and Technology Center	
Attn: J. F. Crider (Code FSTC/DRXST-MTI)	1
220 7th Street	
Charlottesville, VA 22901	

DISTRIBUTION (Cont.)

	Copies
Army Materials & Mechanics Research Center	
Attn: J. J. DeMarco	1
J. W. McCauley	1
A. Levitt	1
J. Greenspan	1
F. Larson	1
L. R. Aronin	1
Watertown, MA 02172	
Army Material Development and Readiness Command	
Attn: J. W. Crellin (Code DRCDE-L)	1
5001 Eisenhower Avenue	
Alexandria, VA 22333	
Army Mobility Equipment R&D Command	
Attn: J. Sullivan (Code DRXFB)	1
G. D. Farmer, Jr. (Code DRDME-VM)	1
Dr. J. R. Huff (Code DRDME-EC)	1
Electrochemical Division	
Fort Belvoir, VA 22060	
Army Research Office	
Attn: B. F. Spielvogel	1
J. C. Hurt	1
P.O. Box 12211	
Research Triangle Park, NC 27709	
Army Scientific Liaison & Advisory Group	
Attn: HQDA (DAEN-ASR-SL)	1
Washington, DC 20314	
Ballistic Missile Defense Officer	
BMD-ATC	
Attn: M. L. Whitfield	1
P.O. Box 1500	
Huntsville, AL 35807	

	Copies
Office of Chief of Research & Development	
Attn: Dr. S. J. Magram	1
Department of the Army	
Energy Conversion Branch	
Room 410, Highland Building	
Washington, DC 20315	
Air Force Flight Dynamics Laboratory	
Attn: D. Roselius	1
L. Kelley	1
Wright-Patterson Air Force Base	
Dayton, OH 45433	
AF Weapons Laboratory	
Attn: Charles Stein	1
Kirtland AFB	
Albuquerque, NM 87115	
Air Force Wright Aeronautical Laboratory	
Attn: M. Duhl (Code MB)	1
T. Ronald (Code LLS)	1
W. S. Bishop (Code POOC-1)	1
R. M. Neff (Nonmetellic Mat. Div.)	1
D. R. Beeler (Code MB)	1
D. Marsh (Electrochemistry Code POOC-1)	1
Wright-Patterson AFB, OH 45433	
Frank J. Seiler Research Laboratory, AFSC	
Attn: LTCOL Lowell A. King (Code FJSRL/NC)	1
USAF Academy, CO 80840	
SD/YLXT	
Attn: MAJ R. Gajewski	1
P.O. Box 92960, WPC	
Los Angeles, CA 90009	
Central Intelligence Agency	
Attn: C. Scuilla	1
G. Methlie	1
Washington, DC 20505	

DISTRIBUTION (Cont.)

	Copies
Department of Energy Attn: Dr. A. Landgrebe (Code MS E-463) Division of Applied Technology Washington, DC 20545	1
Department of Energy Attn: L. J. Rogers (Code 2101) Division of Electric Energy Systems Washington, DC 20545	1
NASA Scientific and Technical Information Facility Attn: Library P.O. Box 33 College Park, MD 20740	1
National Bureau of Standards Metallurgy Division Inorganic Materials Division Washington, DC 20234	1
NASA Lewis Research Center Attn: Mr. R. A. Signorelli	1
J. S. Fordyce (Code MS 309-1)	1
H. J. Schwartz (Code MS 309-1) Cleveland, OH 44135	1
NASA Goodard Space Flight Center Attn: G. Halpert (Code 711) Greenbelt, MD 20771	1
NASA Headquarters Attn: M. Greenfield (Code RTS-6)	1
Dr. J. H. Ambrus 600 Independence Avenue Washington, DC 20546	1

	Copies
NASA/Langley Research Center Attn: E. Mathauser (Code MS188A)	1
Dr. T. Bales	1
Dr. D. Tenney Hampton, VA 23365	1
General Electric Company Attn: Kenneth J. Hall Re-entry Systems Operations P. O. Box 7722 Philadelphia, PA 19101	1
LTJG F. P. Flight Helicopter Anti-Submarine Squardron #5 FPO Miami, FL 34099	1
Ms. A. L. Lee 3004 Castleleigh Road Silver Spring, MD 20904	1
Internal Distribution:	
E431	9
E432	3
R04 (D. L. Love)	1
R30 (J. R. Dixon)	1
R32 (R. A. Sutula)	1
R32 (W. A. Ferrando)	10
R32 (Staff)	5
R33 (C. E. Mueller)	1

END

FILMED

10-84

DTIC